(Received 29 June 2025, Accepted 29 July 2025, Scheduled 6 August 2025)

Energy-Based Adaptive Krylov Subspace Basis Functions Method for Solving Bistatic Scattering Problems

Jianhao Xiang[1], Zhonggen Wang[1,*], Haoran Yuan[1], and Wenyan Nie[2]

[1] School of Electrical and Information Engineering, Anhui University of Science and Technology, Huainan 232001, China
[2] School of Mechanical and Electrical Engineering, Huainan Normal University, Huainan, 232001, China

ABSTRACT: To address the convergence inefficiency of the conventional CS-Krylov-block method in solving electromagnetic scattering problems, this paper presents an adaptive Krylov subspace basis function method (AKSBFM) based on spectral energy thresholds. In this method, Krylov subspace basis functions (KSBFs) are first generated within each extended subdomain using localized self-impedance matrices. Singular value decomposition (SVD) is performed on the candidate basis set to evaluate energy contributions, and only the dominant components exceeding a predefined energy threshold are retained. As a result, the number of basis functions per subdomain is automatically adjusted, and a compact, well-conditioned reduced matrix system is constructed. This energy-guided truncation significantly eliminates redundant modes, yielding improved numerical stability and reducing the condition number by up to two orders of magnitude. Numerical experiments demonstrate that, compared with the traditional CS-Krylov-block method AKSBFM improves computational efficiency while ensuring computational accuracy.

1. INTRODUCTION

The method of moments (MoM) is a classical numerical technique for solving electromagnetic scattering problems [1, 2]. It transforms surface integral equations into dense impedance matrix equations through spatial discretization, enabling the computation of induced current distributions on conducting surfaces under external excitations. However, as the electrical size of the target increases, conventional MoM becomes impractical due to the prohibitive cost of storing and solving large-scale full-rank matrices. To address this challenge, a variety of acceleration techniques have been proposed, including the fast multipole method (FMM) [3], multilevel fast multipole algorithm (MLFMA) [4], conjugate gradient fast Fourier transform (CG-FFT) [5], adaptive integral method (AIM) [6], and adaptive cross approximation (ACA) [7].

In recent years, compressed sensing (CS) [8] has been incorporated into the MoM to develop novel numerical techniques for solving electromagnetic scattering problems. These CS-MoM approaches can be broadly categorized into monostatic and bistatic scattering configurations. In CS-MoM techniques, sparse bases such as characteristic basis functions (CBFs) [9], characteristic modes (CMs) [10], and Krylov subspace basis functions (KSBFs) [11] are commonly employed. Unlike CBFs and CMs, which are derived through mode decomposition, KSBFs are constructed iteratively, making them suitable for electromagnetic problems with arbitrary geometric complexity. In conventional methods such as CS-Krylov, the generation of KSBFs requires access to a fully populated impedance matrix [12–14]. The iterative process involves repeated matrixvector multiplications based on row sampling, which becomes computationally expensive when dealing with large-scale matrices. To alleviate this issue, a block-based variant, namely CS-Krylov-block method, has been proposed [15]. This method leverages the self-immediate of each subdomain block to construct local KSBFs, significantly improving computational efficiency. Despite its advantages, the CS-Krylov-block method assigns a fixed number of basis functions to each subdomain based on prior knowledge, adopting a uniform allocation strategy. This approach fails to account for spatial variations in electromagnetic response. Subdomains with complex geometrical features or field singularities typically require more basis functions to achieve accurate representation, while smoother regions can be sufficiently described using fewer modes [16–18]. Consequently, the fixed allocation scheme leads to underfitting in critical regions and redundant computation in simpler areas, ultimately reducing overall reconstruction accuracy and computational efficiency.

To address the limitations of fixed basis allocation strategies, this paper proposes an adaptive Krylov subspace basis functions method (AKSBFM) based in spectral energy analysis. Initially, candidate basis functions are generated within each extended subdomain. In each extended subdomain, candidate basis functions are first generated and evaluated using singular value decomposition (SVD) [19] to analyze their energy distribution. A subset of basis functions with the highest energy contributions is then selected according to a predefined energy threshold, resulting in a compact and stable local representation. This strategy avoids the redundancy and underfitting issues caused by uniform basis allocation in the conventional CS-Krylov-block method, thereby improving numerical stability and solution accuracy. Under identical block partitioning and compression ratio conditions, the proposed method exhibits

* Corresponding author: Zhonggen Wang (zgwang@ahu.edu.cn).

better orthogonality and sensitivity to numerical rank, effectively mitigating the ill-conditioning and performance degradation commonly encountered in fixed-dimension schemes.

This paper is organized as follows. Firstly, in Section 1, the theory of the proposed method is elaborated. Then, in Section 2, the complexity of the proposed method was analyzed, and in Section 3, the proposed method was further verified through numerical experiments. Finally, the conclusion is presented in Section 4.

1.1. Traditional CS-Krylov-block Method

When using the MoM to solve electromagnetic scattering problems, the Rao-Wilton-Glisson (RWG) basis function is used to discretize the current to be solved. For perfect electric conducting (PEC) geometries, the application of the MoM formulation to the electric field integral equation led to a dense, complex linear system of the form:

$$\mathbf{Z}_{(N\times N)}\mathbf{I}_{(N\times 1)} = \mathbf{V}_{N\times 1} \tag{1}$$

where $\mathbf{Z}$, $\mathbf{I}$ and $\mathbf{V}$ are the impedance matrix, unknown current vector, and voltage vector, respectively, and N is the total number of RWG basis functions. The elements of $\mathbf{Z}$ and $\mathbf{V}$ are computed by using the following equation:

$$Z_{pq} = jk\eta \int_s \int_{s'} G \left(\mathbf{f}_p(\mathbf{r})\cdot\mathbf{f}_q(\mathbf{r}') - \frac{1}{k^2}\nabla_s\cdot\mathbf{f}_p(\mathbf{r})\nabla'_s\cdot\mathbf{f}_q(\mathbf{r}')\right)d\mathbf{r}d\mathbf{r}' \tag{2}$$

$$V_p = \int_s \mathbf{f}_p(\mathbf{r})\cdot\mathbf{E}^i(\mathbf{r})d\mathbf{r} \tag{3}$$

where k, η, and G are the wavenumber, impedance, and Green's function in free space, respectively, $\mathbf{f}_p(\mathbf{f}_q)$ is the $p_{th}(q_{th})$ RWG basis functions, and $\mathbf{E}^i(\mathbf{r})$ is the incident electric field. In [20], the object is typically divided into different subdomains. However, this partitioning alters the shape of the object, leading to discontinuities in the surface current distribution. To address this issue, each subdomain is extended to ensure the smoothness and continuity of the characteristic currents near the virtual boundaries.

The initial object is segmented into several subdomains, whose number is calculated by $R = 0.9N^{1/3}$ [21], where R represents the number of subdomains, therefore, can be converted to:

$$\begin{bmatrix} \mathbf{Z}_{11} & \mathbf{Z}_{12} & \cdots & \mathbf{Z}_{1R} \\ \mathbf{Z}_{21} & \mathbf{Z}_{22} & \cdots & \mathbf{Z}_{2R} \\ \vdots & \vdots & \cdots & \vdots \\ \mathbf{Z}_{R1} & \mathbf{Z}_{R2} & \cdots & \mathbf{Z}_{RR} \end{bmatrix} \begin{bmatrix} \mathbf{J}_1 \\ \mathbf{J}_2 \\ \vdots \\ \mathbf{J}_R \end{bmatrix} = \begin{bmatrix} \mathbf{V}_1 \\ \mathbf{V}_2 \\ \vdots \\ \mathbf{V}_R \end{bmatrix} \tag{4}$$

where $\mathbf{Z}_{mm}$ denotes the self-impedance matrix of dimension $N_m \times N_m$, $\mathbf{Z}_{mn}(m,n=1,2,\ldots,R; m\neq n)$ represents the mutual impedance matrix of dimension $N_m \times N_n$, N_m is the number of unknowns on subdomain m and N_n is the number of unknowns on subdomain n, respectively. $\mathbf{J}_m$ and $\mathbf{V}_m$ represent the present current coefficient vector and the excitation vector for subdomain m, respectively; $\mathbf{J}_m$ and $\mathbf{V}_m$ have the same size of $N_m \times 1$.

In [15], the measurement matrix $\mathbf{Z}_s$ and the measured values vector $\mathbf{V}_s$ are constructed by unform sampling s rows from Z and $\mathbf{V}$ respectively, thus (1) is transformed into an underdetermined system as:

$$\mathbf{Z}_s\mathbf{I} = \mathbf{V}_s \tag{5}$$

Since sub-subdomain leads to discontinuities in the edge currents, it is necessary to extend a certain distance on each block as a buffer and then construct the KSBFs on each block separately, which can be mathematically expressed by:

$$\mathbf{K}^{i,e}_{k_b}(\mathbf{Z}^e_{ii}, \mathbf{V}^e_{ii}) = \mathrm{span}\{\mathbf{V}^e_i, \mathbf{Z}^e_{ii}\mathbf{V}^e_i, (\mathbf{Z}^e_{ii})^2\mathbf{V}^e_i, \ldots, (\mathbf{Z}^e_{ii})^{k_b-1}\mathbf{V}^e_i\} \tag{6}$$

in which the superscript e is the extension symbol, k_b is the number of basis functions after blocking.

By using Arnoldi procedure and partial orthogonal method accelerate generating a set of partially orthogonal basis:

$$\mathbf{J}^{(i)} = \begin{bmatrix} \mathbf{J}^i_1 & \mathbf{J}^i_2 & \cdots & \mathbf{J}^i_{k_b} \end{bmatrix} \tag{7}$$

Therefore, the overall basis function is:

$$\mathbf{\Psi}_{\text{Krylov}} = \begin{bmatrix} \mathbf{J}^{(1)} & \mathbf{J}^{(2)} & \cdots & \mathbf{J}^{(R)} \end{bmatrix} \tag{8}$$

$\mathbf{\Psi}_{\text{Krylov}}$ acts as a change-of-basis operator that projects the current coefficients $\mathbf{I} \in \mathrm{C}^{N\times 1}$ into a lower-dimensional, spares domain:

$$\mathbf{I} \approx \mathbf{\Psi}_{\text{Krylov}}\boldsymbol{\alpha} \tag{9}$$

where $\boldsymbol{\alpha} \in \mathrm{C}^{K\times 1}$ is a spares coefficient vector and $K = \sum_{i=1}^{R} k_b^{(i)}$ is the total number of basis vector across all blocks.

Substitute (9) into (5), we can obtain:

$$\mathbf{Z}_s\mathbf{\Psi}_{\text{Krylov}}\boldsymbol{\alpha} = \mathbf{A}\boldsymbol{\alpha} = \mathbf{V}_s \tag{10}$$

where $\mathbf{A}$ is the recovery matrix. The sparse coefficient vector $\boldsymbol{\alpha}$ can be obtained by the least square (the superscript T indicates transposition):

$$\min_{\alpha} \|\mathbf{A}\boldsymbol{\alpha} - \mathbf{V}_s\|_2^2 \quad \text{subject to} \quad \boldsymbol{\alpha} = \left(\mathbf{A}^T\mathbf{A}\right)^{-1}\mathbf{A}^T\mathbf{V}_s \tag{11}$$

However, as the number of unknowns increases, the CS-Krylov-block method must partition the geometry into more extended subdomains to maintain accuracy, while assigning the same number of basis functions to each block. This uniform allocation strategy results in two major issues: redundancy in electrically smooth regions and insufficiency in geometrically complex areas, both of which degrade computational efficiency and numerical stability.

1.2. Proposed Method

To alleviate this limitation, we have introduced a construction scheme for adaptive Krylov basis functions. In this method, SVD is applied to the KSBFs matrix. The singular values of the principal energy direction reflect the contribution of each direction to the overall energy. By constructing an accumulated energy curve and setting an energy threshold, the minimum number of KSBFs required to retain the key information

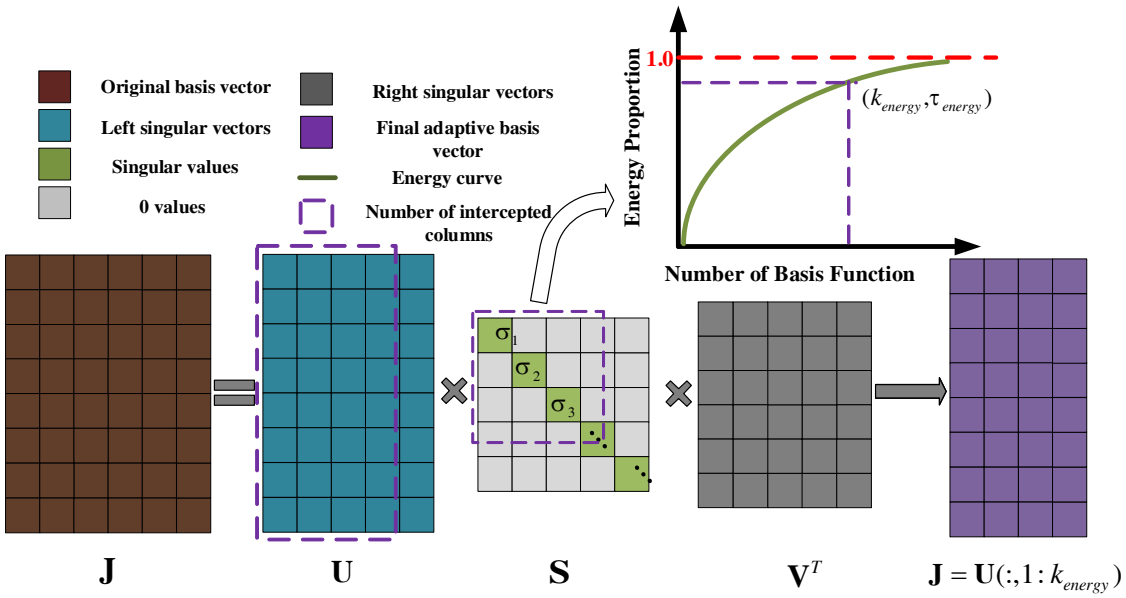

FIGURE 1. Construction of final adaptive basis functions guided by cumulative spectral energy.

can be determined. The complete schematic diagram is shown in Figure 1.

The standard Krylov subspace method is based on iterative generation of basis functions using matrix-vector multiplications. For a given subdomain i, the basis functions are derived from an extended matrix $\mathbf{J}^{(i)} \in \mathrm{C}^{N_i \times k_b}$, which is decomposed using SVD:

$$\mathbf{J}^{(i)} = \mathbf{U}^{(i)}\mathbf{S}^{(i)}\mathbf{V}^{(i)T} \tag{12}$$

where $\mathbf{U}^{(i)}$ and $\mathbf{V}^{(i)T}$ are both orthogonal matrixes, and $\mathbf{S}^{(i)}$ is a diagonal matrix whose elements are arranged from the largest to the smallest with a rapid decay trend, all which are singular values of $\mathbf{J}^{(i)}$. Then Calculate the energy distribution based on the squares of these singular values. Then, calculate the cumulative energy of the singular values and normalize it to the total energy as follows:

$$E_k^{(i)} = \sum_{j=1}^{k} \sigma_j^2 \Big/ \sum_{j=1}^{k_b} \sigma_j^2 \tag{13}$$

where $E_k^{(i)}$ represents the energy proportion of the basis function retained in the i block $\sum_{j=1}^{k} \sigma_j^2$ and $\sum_{j=1}^{k_b} \sigma_j^2$ denote the total energy contributed by the first k basis functions and the combined energy of all k_b basis functions, respectively. To adaptively select the number of basis functions, we introduce an energy threshold $\tau_{energy} \in (0, 1)$ The number of basis functions $k_{energy}^{(i)}$ is selected such that the cumulative energy exceeds the threshold τ_{energy}:

$$k_{energy}^{(i)} = \min\left\{k | E_k^{(i)} \geq \tau_{\text{energy}}\right\} \tag{14}$$

Then, the retained basis functions can be expressed as:

$$\widehat{\mathbf{J}}^{(i)} = \mathbf{U}^{(i)}(:, 1 : k_{energy}^{(i)}) \tag{15}$$

After obtaining the KSBFs on all blocks, the sparse basis is constructed as follows:

$$\widehat{\mathbf{\Psi}}_{\text{Krylov}} = [\ \widehat{\mathbf{J}}^{(1)} \quad \widehat{\mathbf{J}}^{(2)} \quad \cdots \quad \widehat{\mathbf{J}}^{(R)}\ ] \tag{16}$$

Substituting (16) to (10), the CS model can be constructed as $\mathbf{Z}_s\widehat{\mathbf{\Psi}}_{\text{Krylov}}\widehat{\alpha} = \mathbf{V}_s$. $\widehat{\boldsymbol{\alpha}}$ is obtained by employing least-square and substituting into (9), which will lead to the final current on the object's surface.

From the above theory, the number of KSBFs decreased from $\sum_{i=1}^{R} k_b^{(i)}$ to $\sum_{i=1}^{R} k_{energy}^{(i)}$, which significantly shortened the time required for calculating the current. Furthermore, through the improvement of SVD, the redundancy among KSBFs was eliminated, and the orthogonality among sub-block basis functions was enhanced. The condition number of recovery matrix $\mathbf{Z}_s\mathbf{\Psi}_{\text{Krylov}}$ was improved, thereby further enhancing the stability of the data.

In summary, the proposed adaptive Krylov subspace method maintains a reconstruction accuracy comparable to the traditional fixed-order approach, but with notable improvements in computational efficiency and numerical stability. By adjusting the number of basis functions for each block according to the dynamic energy, the method avoids unnecessary redundancy in smooth regions while ensuring sufficient expressiveness in complex areas. Moreover, the adaptively selected bases exhibit better orthogonality, reducing the risk of ill-conditioning that commonly arises in fixed-dimensional formulations. These benefits lead to a more compact solution representation and more stable compressed sensing recovery.

2. COMPLEXITY ANALYSIS

The main innovation of this study lies in combining the SVD algorithm based on energy extraction and error determination with CS-Krylov method to obtain numerically stable basis func-

tions, which can better represent the target current. Therefore, it is sufficient to analyze the complexity of constructing the basis functions and the complexity of the least squares method.

2.1. Krylov Basis Function Construction

In the traditional method, a fixed number of Krylov basis vectors k_b is constructed per block. Each vector requires one matrix-vector multiplication and orthogonalization, the complexity of this part is $O(R \cdot (N/R)^2 \cdot k_b) = O((N^2 \cdot k_b)/R)$; In the adaptive method, the number of basis vectors $k^{(i)}$ is selected dynamically for each block. Let $\bar{k} = (\sum_{i=1}^{R} k_{energy}^{(i)})/R$ denote the average number of retain vectors. The total complexity becomes $O((N^2 \cdot \bar{k})/R) + O(N \cdot \bar{k}^2)$, the first term corresponding to Krylov generation and orthogonalization; the second term is the cost of selecting the basis functions.

2.2. Least-squares Recovery

In the reconstruction phase, both methods use a least-squares solver instead of sparse recovery algorithms. Let s be the number of sampled rows in $\mathbf{Z}_s$, and K the total number of basis vector. In the traditional method, $K = R \cdot k_b$; In the proposed method, $K = \sum_{i=1}^{R} k_{energy}^{(i)}$. Therefore, the complexity of the least squares method is $O(s \cdot K^2 + K^3)$. The first term represents matrix multiplications, and the second term is the cost of solving a small linear system. Since K is typically much smaller than in the proposed method, it is more efficient in this as well.

In summary, compared to CS-Krylov-block, the AKSBFM requires more time during the basis function construction phase, but spends less time during the current coefficient recovery phase. Ultimately, the total computational time is lower than that of CS-Krylov-block.

3. NUMERICAL RESULTS

This section validates the effectiveness of AKSBFM through two numerical examples, with the root mean square error (RMSE) of bistatic RCS adopted as the accuracy metric, defined as:

$$\mathrm{RMSE} = \sqrt{\frac{1}{N_a}\sum_{i=1}^{M}\left|\boldsymbol{\sigma}_{\mathbf{X},\mathbf{i}} - \boldsymbol{\sigma}_{\mathbf{ref},\mathbf{i}}\right|^2} \tag{17}$$

where N_a represents the sample number, $\boldsymbol{\sigma}_{\mathbf{X},\mathbf{i}}$ and $\boldsymbol{\sigma}_{\mathbf{ref},\mathbf{i}}$ denote the calculation results of the method used and MoM, respectively.

3.1. Perfect Electrical Conductor Sphere

To demonstrate the effectiveness of the AKSBFM, a numerical experiment is conducted on a perfect electric conductor (PEC) sphere with a diameter of 0.8 m. The sphere is illuminated by a plane wave with a polarization angle of 90 degrees at a center frequency of 700 MHz. The surface of the object is discretized using RWG basis functions, resulting in 15,370 triangles and 23,055 unknowns.

To quantitatively investigate the influence of the energy threshold on the number of retained basis functions in each block, Figure 2 illustrates the adaptive truncation results across eight blocks under different threshold levels. Each color corresponds to a specific energy threshold value. As the energy threshold increases, a large portion of the singular value spectrum must be retained, resulting in a greater number of basis functions preserved per block. When the threshold is set to 1.0, no truncation is applied, and all initially generated basis vectors are retained. In contrast, lower thresholds allow significant dimensionality reduction, especially in geometrically simpler regions, by discarding low-energy modes that contribute marginally to the local subspace representation.

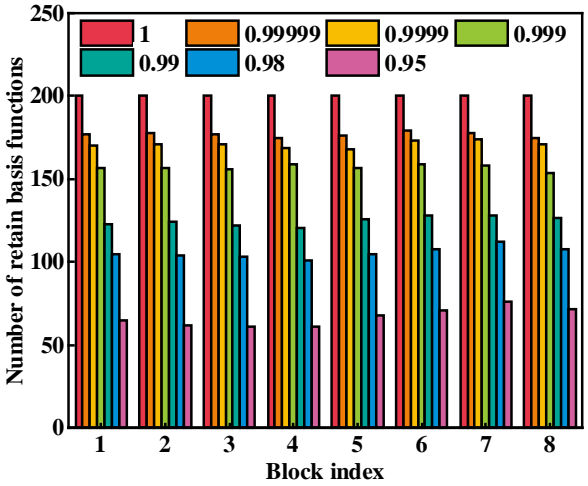

FIGURE 2. Effect of energy threshold on basis function retention for a PEC sphere.

To evaluate the influence of the energy threshold on numerical performance, Figure 3. illustrates the variation trends of solution time and RMSE under different energy threshold values. It can be observed that as the energy threshold increases, the RMSE consistently decreases, indicating that retaining more high-energy basis functions helps to improve solution accuracy. However, when the energy threshold increases from 0.9999 to 1.0, the improvement in RMSE becomes negligible, while the solution time rises sharply. This suggests that further increasing the basis functions offers limited accuracy gains but leads to a significant increase in computational cost. Therefore, an energy threshold of 0.9999 is selected as the optimal choice, achieving a balanced trade-off between accuracy and efficiency.

To further validate the numerical stability of the proposed method, Table 1 presents the condition numbers of the recovery matrix $\mathbf{Z}_s\boldsymbol{\Psi}_{\mathrm{Krylov}}$ for varying numbers of subdomains for both the traditional and proposed Krylov methods. As the number of subdomains increases, the fixed-order Krylov approach exhibits a rapid growth in the condition number, rising from 192.41 to $2.88E+09$. This is due to the increasing linear dependency among the basis functions as the subdomains become

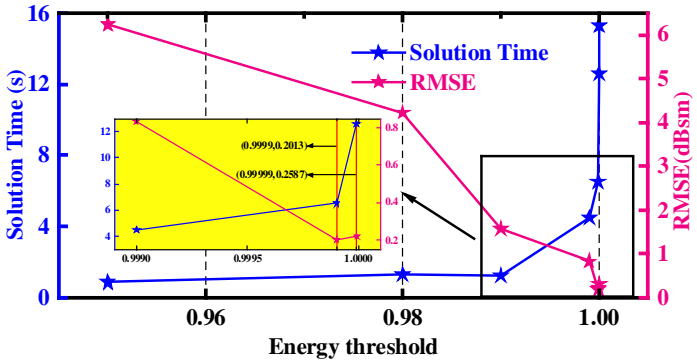

FIGURE 3. Influence of energy threshold on solution time and RMSE for a PEC sphere.

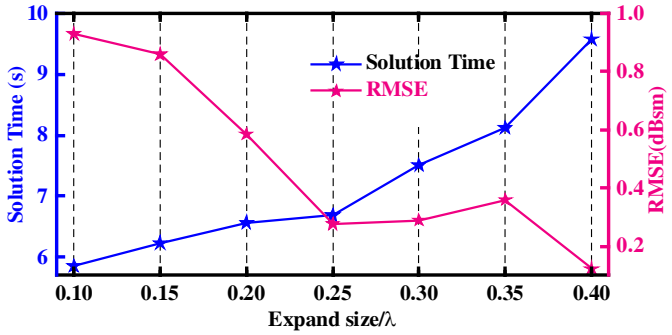

FIGURE 4. Influence of expansion size on solution time and RMSE for a PEC sphere.

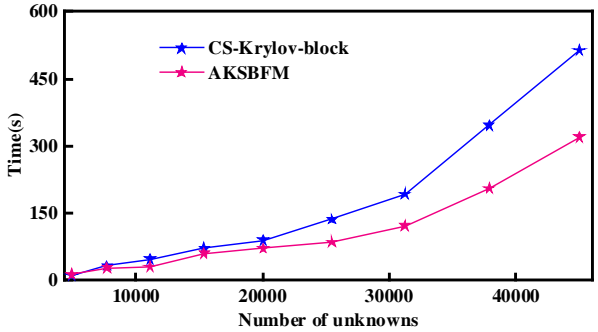

FIGURE 5. Time comparison with different unknowns.

TABLE 1. Comparison of condition numbers between CS-Krylov-block and AKSBFM.

Block number	CS-Krylov-block	AKSBFM
8	192.41	109.99
12	211.33	92.62
15	876.66	97.13
20	1.10E+05	134.02
24	2.88E+09	1520.21

smaller. In contrast, the proposed adaptive Krylov method maintains relatively low condition numbers, with a maximum value of only 1520.21. This indicates better numerical stability. The results clearly demonstrate the robustness of adaptive basis selection in preventing redundancy and maintaining orthogonality, particularly when the spatial partitioning is finer.

To verify the influence of different subdomains extension sizes on solution time and RMSE, Figure 4 shows the variation of these metrics for a PEC sphere as the expansion size is from 0.10λ to 0.40λ. As the expansion size increases, the solution time shows an increasing trend. In contrast, the RMSE decreases, indicating improved numerical accuracy due to enhanced continuity at subdomain interfaces. These opposing trends highlight a typical trade-off between computational efficiency and approximation accuracy. When the expansion size reaches approximately 0.25λ, the RMSE is significantly reduced while the solution time remains moderate, suggesting that this setting offers a favorable compromise for practical applications.

To demonstrate the effectiveness of AKSBFM in current reconstruction, Figure 5 presents the surface current magnitude distributions obtained by (a) MoM, (b) CS-Krylov-block, and (c) AKSBFM. All results are shown using a unified color scale. It can be observed that the proposed method accurately preserves the primary energetic structures consistent with the MoM solution, while avoiding the numerical artifacts seen in the CS-Krylov-block result. Notably, smoother current transitions and enhanced local continuity can be observed in the proposed result, especially in high-gradient regions. This confirms the advantage of the proposed method in basis compactness and numerical stability, achieved by adaptively selecting dominant response components in each subdomain.

Further, the effectiveness of the proposed method is studied. The bistatic RCS of the sphere is calculated using CS-Krylov-block and AKSBFM at different incident wave frequencies, respectively. A comparison of their simulation time is shown in Figure 5. Obviously, the increase in frequency means a large electrical size and more unknowns. As shown in Figure 5, the time consumption of AKSBFM increases at a slower rate as the number of unknown variables increases.

In summary, the PEC sphere is divided into 8 blocks, and each block is expanded by 0.25λ, resulting in an expanded system with 25,684 unknowns. In the conventional KSBFM approach, a fixed number of 200 basis functions are assigned to each block based on prior knowledge, leading to a total of 1,600 KSBFs. In contrast, the proposed AKSBFM adaptively selects the number of basis functions for each block using a spectral energy threshold of 0.9999. Moreover, the number of newly

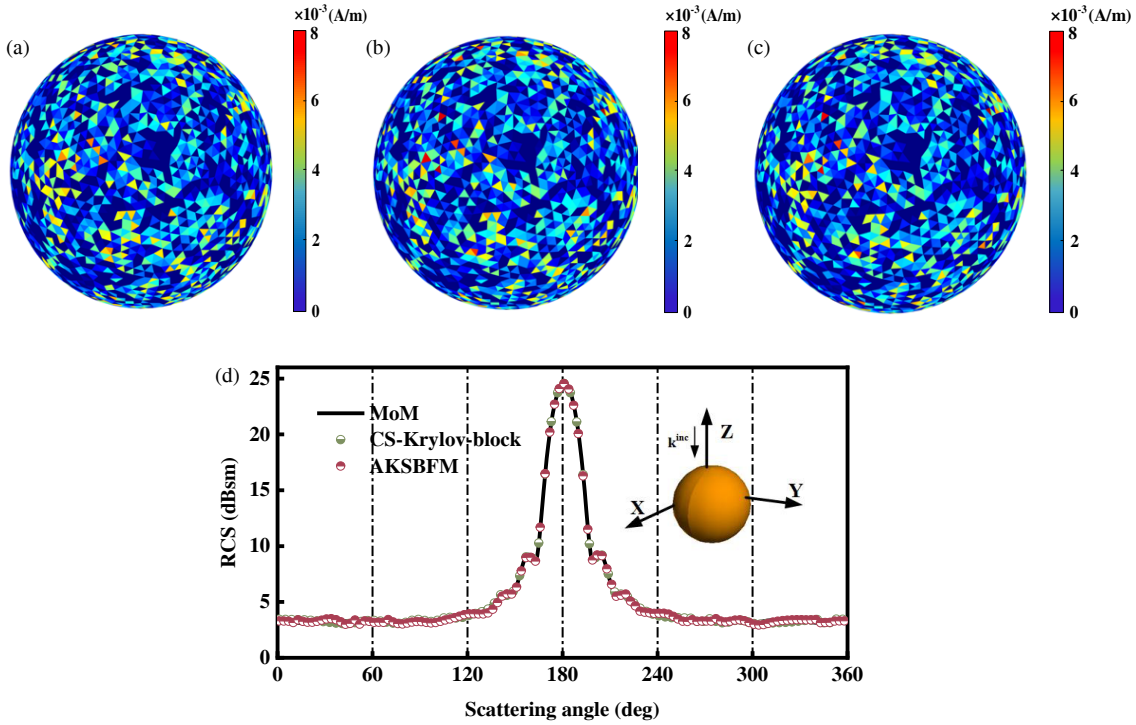

FIGURE 6. (a) Surface current by MoM. (b) Result of CS-Krylov-block. (c) Result of AKSBFM. (d) Bistatic RCS of PEC sphere at 700 MHz.

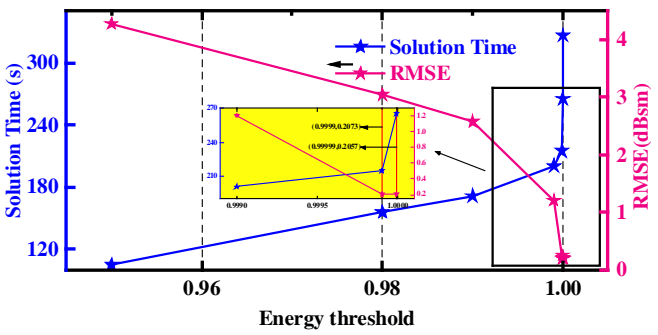

FIGURE 7. Influence of energy threshold on solution time and RMSE for a PEC array target.

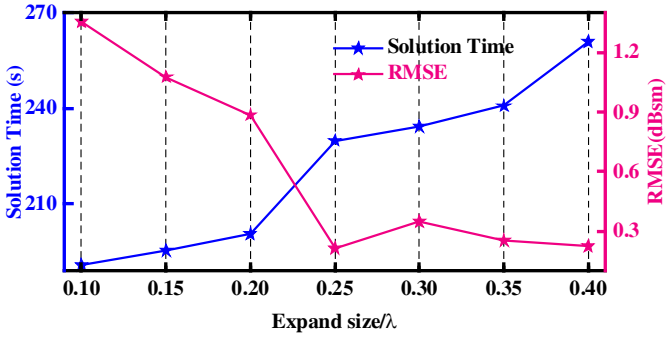

FIGURE 8. Influence of expansion size on solution time and RMSE for a PEC array target.

generated vectors and the number of partially generated vectors from earlier periods were set to 100 and 80, respectively. Consequently, only 1103 basis functions are retained, representing a significant reduction in the number of basis functions. Figure 6 presents the RCS results computed using MoM, CS-Krylov-block, and AKSBFM. Both CS-Krylov-block and AKSBFM maintain a high degree of accuracy when compared to MoM, with AKSBFM achieving the same level of accuracy using a substantially smaller basis set, demonstrating its efficiency and adaptivity.

3.2. Perfect Electrical Conductor Array Target

To further validate the effectiveness of the proposed method on more complex geometries, the RCS of an array target composed of 36 PEC objects of two different shapes is computed using MoM, CS-Krylov-block, and AKSBFM. The incident wave frequency is set to 800 MHz, and the target surface is discretized into 51984 triangular facets, resulting in a total of 77976 unknowns. The target is uniformly divided into 36 subdomains. We analyzed the array target using different energy thresholds and subdomain expansions, as shown in Figures 7 and 8. We chose an energy threshold of 0.9999 and a subdomain expansion of 0.25λ. For the CS-Krylov-block approach, 400 basis functions are assigned to each subdomain, resulting in a total of 14,400 KSBFs. As a result, the number of retained basis functions is reduced to 9,150, demonstrating a significant reduction compared to the CS-Krylov-block. The numerical results are shown in Figure 9, indicate thar AKSBFM agrees well with the MoM solution in both current distribution and RCS accuracy.

To further demonstrate the effectiveness of the proposed method, the peak resident memory of CS-Krylov-block and

TABLE 2. Summary of sparse basis and recovery matrix memory usage.

Model	Method	Sparse basis matrix memory (G)	Recovery matrix memory (G)
Sphere	CS-Krylov-block	0.61	0.31
	AKSBFM	0.42	0.21
Array target	CS-Krylov-block	16.47	8.36
	AKSBFM	10.63	5.31

TABLE 3. The simulation time of different processes.

Model	Unknowns	Method	Basis functions construction time (s)	Solving time (s)	Total time (s)
Sphere	25684	CS-Krylov-block	56.27	15.28	71.55
		AKSBFM	60.21	6.32	66.53
Array target	77976	CS-Krylov-block	367.51	502.41	862.92
		AKSBFM	402.87	210.14	613.01

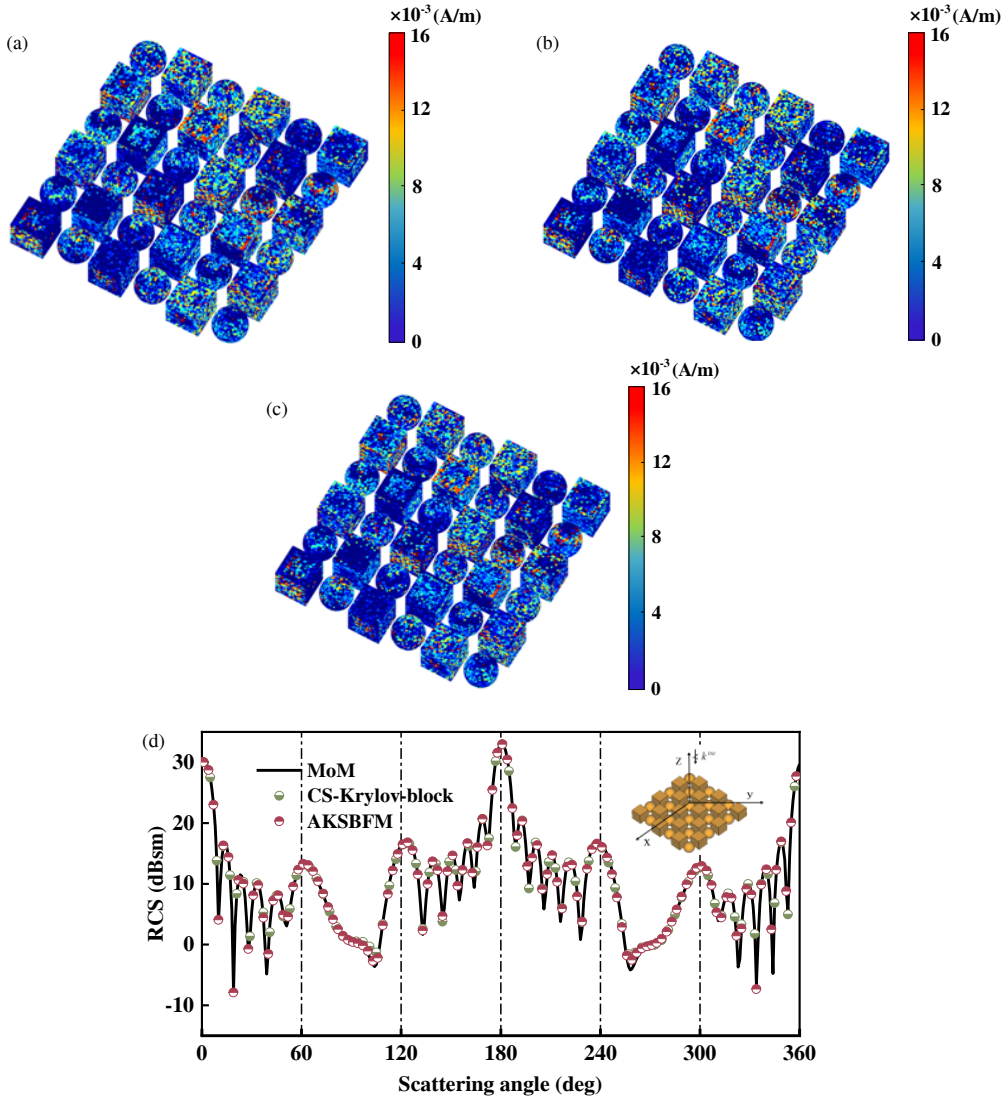

FIGURE 9. (a) Surface current by MoM. (b) Result of CS-Krylov-block. (c) Result of AKSBFM, (d) Bistatic RCS of the array target at 800 MHz.

AKSBFM in double precision is also evaluated. It mainly stores the data from the sparse basis $\mathbf{\Psi}_{\text{Krylov}} \in \mathrm{C}^{N\times K}$ and recovery matrix $\mathbf{Z}_s\mathbf{\Psi}_{\text{Krylov}} \in \mathrm{C}^{s\times K}$. As shown in Table 2, the proposed AKSBFM method reduces the memory footprint.

Table 3 lists the time consumption corresponding to Figures 6 and 9. Compared with CS-Krylov-block, AKSBFM significantly accelerated the solution process by 58.6% and 58.2%, respectively, in terms of current solution time. Although AKSBFM spent more time generating the basis functions than CS-Krylov-block, the total time was shortened by 7.1% and 28.9%, respectively. In terms of time, the proposed method is superior to CS-Krylov-block, and it improves computational efficiency in the solving stage while maintaining accuracy.

4. CONCLUSION

In this paper, adaptive Krylov subspace basis functions method (AKSBFM) is proposed to analyze Bistatic scattering problems. By introducing spectral energy threshold and SVD techniques, AKSBFM can dynamically optimize the number of basis functions in each subregion, reduce redundant calculations, and enhance the orthogonality between basis functions. Numerical experiments using PEC sphere and missile models as examples have confirmed the advantages of AKSBFM in improving computational efficiency and numerical stability. The results show that compared with the traditional CS-Krylov-block method, AKSBFM improves computational efficiency while ensuring accuracy. Although the proposed AKSBFM method demonstrates improved numerical stability and computational efficiency, it also introduces additional implementation challenges. In particular, the blocklevel SVD preprocessing and the irregular data structures arising from adaptive basis selection may increase the coding complexity and require careful memory management during practical applications.

ACKNOWLEDGEMENT

This work was supported in part by the Natural Science Foundation of Anhui Provincial Education Department under Grant No. 2022AH051583, in part by the National Natural Science Foundation of China under Grant No. 61401003, in part by the Anhui Province Graduate Academic Innovation Project under grant No. 2024cx2062.

REFERENCES

[1] Harrington, R. F., "Field computation by moment methods," *The Macmillan Comp.*, Vol. 130, No. 6, 276–280, 1968.

[2] Burke, G. J., E. K. Miller, S. Chakrabarti, and K. Demarest, "Using model-based parameter estimation to increase the efficiency of computing electromagnetic transfer functions," *IEEE Transactions on Magnetics*, Vol. 25, No. 4, 2807–2809, Jul. 1989.

[3] Coifman, R., V. Rokhlin, and S. Wandzura, "The fast multipole method for the wave equation: A pedestrian prescription," *IEEE Antennas and Propagation Magazine*, Vol. 35, No. 3, 7–12, Jun. 1993.

[4] Hu, J., Z. Nie, X. Que, and M. Meng, "Fast computation of scattering from 3D complex structures by MLFMA," *Journal of Systems Engineering and Electronics*, Vol. 19, No. 5, 872–877, Oct. 2008.

[5] Xu, X. M. and Q. H. Liu, "Fast spectral-domain method for acoustic scattering problems," *IEEE Transactions on Ultrasonics, Ferroelectrics, and Frequency Control*, Vol. 48, No. 2, 522–529, Mar. 2001.

[6] Nie, X. C., N. Yuan, L. W. Li, and Y. B. Gan, "Fast analysis of RCS over a frequency band using pre-corrected FFT/AIM and asymptotic waveform evaluation technique," *IEEE Transactions on Antennas and Propagation*, Vol. 56, No. 11, 3526–3533, Nov. 2008.

[7] Zhao, K., M. N. Vouvakis, and J.-F. Lee, "The adaptive cross approximation algorithm for accelerated method of moments computations of EMC problems," *IEEE Transactions on Electromagnetic Compatibility*, Vol. 47, No. 4, 763–773, Nov. 2005.

[8] Donoho, D. L., "Compressed sensing," *IEEE Transactions on Information Theory*, Vol. 52, No. 4, 1289–1306, Apr. 2006.

[9] Lucente, E., A. Monorchio, and R. Mittra, "An iteration-free MoM approach based on excitation independent characteristic basis functions for solving large multiscale electromagnetic scattering problems," *IEEE Transactions on Antennas and Propagation*, Vol. 56, No. 4, 999–1007, Apr. 2008.

[10] Wang, P., Z. Wang, Y. Sun, and W. Nie, "A characteristic mode basis function method for solving wide-angle electromagnetic scattering problems," *Journal of Electromagnetic Waves and Applications*, Vol. 36, No. 14, 1968–1979, Mar. 2022.

[11] Cao, X., M. Chen, Q. Qi, M. Kong, J. Hu, L. Zhang, and X. Wu, "Solving electromagnetic scattering problems by underdetermined equations and Krylov subspace," *IEEE Microwave and Wireless Components Letters*, Vol. 30, No. 6, 541–544, Jun. 2020.

[12] Wang, Z.-G., W.-Y. Nie, and H. Lin, "Characteristic basis functions enhanced compressive sensing for solving the bistatic scattering problems of three-dimensional targets," *Microwave and Optical Technology Letters*, Vol. 62, No. 10, 3132–3138, Oct. 2020.

[13] Brown, P. N. and Y. Saad, "Hybrid Krylov methods for nonlinear systems of equations," *SIAM Journal on Scientific and Statistical Computing*, Vol. 11, No. 3, 450–481, 1990.

[14] Kong, M., M. S. Chen, B. Wu, and X. L. Wu, "Fast and stabilized algorithm for analyzing electromagnetic scattering problems of bodies of revolution by compressive sensing," *IEEE Antennas and Wireless Propagation Letters*, Vol. 16, 198–201, 2017.

[15] Wang, Z., H. Yuan, Y. Sun, W. Nie, and P. Wang, "Block-based Krylov subspace basis functions for solving bistatic scattering problems," *IEEE Antennas and Wireless Propagation Letters*, Vol. 22, No. 10, 2561–2565, Oct. 2023.

[16] Wang, Z., P. Wang, Y. Sun, and W. Nie, "Fast analysis of bistatic scattering problems for three-dimensional objects using compressive sensing and characteristic modes," *IEEE Antennas and Wireless Propagation Letters*, Vol. 21, No. 9, 1817–1821, Sep. 2022.

[17] Park, C.-S., Y.-R. Jeong, I.-P. Hong, and J.-G. Yook, "Block size optimization of CBFM for scattering problems," *IEEE Transactions on Antennas and Propagation*, Vol. 66, No. 10, 5370–5377, Oct. 2018.

[18] Kong, M., M. S. Chen, X. Y. Cao, J. B. Zhu, X. J. Kuang, Q. Qi, and X. L. Wu, "Fast electromagnetic scattering analysis of inhomogeneous dielectric objects over a wide incident angle," *IEEE Antennas and Wireless Propagation Letters*, Vol. 20, No. 8, 1527–1531, Aug. 2021.

[19] Wang, Z., P. Wang, Y. Sun, W. Nie, J. Wu, and H. Lin, "Fast analysis of wideband scattering problems using universal characteristic mode basis functions," *Microwave and Optical Technology Letters*, Vol. 64, No. 11, 1937–1943, Jul. 2022.

[20] Kumar, N., K. J. Vinoy, and S. Gopalakrishnan, "A reduced order model for electromagnetic scattering using multilevel Krylov subspace splitting," in *2015 IEEE International Conference on Computational Electromagnetics*, 341–343, Hong Kong, China, Mar. 2015.

[21] Konno, K., Q. Chen, K. Sawaya, and T. Sezai, "Optimization of block size for CBFM in MoM," *IEEE Transactions on Antennas and Propagation*, Vol. 60, No. 10, 4719–4724, Oct. 2012.